Published in final edited form as:

Hear Res. 2022 December ; 426: 108633. doi:10.1016/j.heares.2022.108633.

Loss of the chromatin remodeler CHD7 impacts glial cells and myelination in the mouse cochlear spiral ganglion

K. Elaine Ritter[a], **Sloane M. Lynch**[b], **Ashley M. Gorris**[b], **Lisa A. Beyer**[c], **Lisa Kabara**[c], **David F. Dolan**[c], **Yehoash Raphael**[c], **Donna M. Martin**[a,d,*]

[a]Department of Pediatrics, University of Michigan Medical School, Ann Arbor, MI, USA

[b]College of Literature, Science and Art, University of Michigan, Ann Arbor, MI, USA

[c]Department of Otolaryngology – Head and Neck Surgery, University of Medical School, Ann Arbor, MI, USA

[d]Department of Human Genetics, University of Michigan Medical School, Ann Arbor, MI, USA

Abstract

CHARGE syndrome is a multiple anomaly developmental disorder characterized by a variety of sensory deficits, including sensorineural hearing loss of unknown etiology. Most cases of CHARGE are caused by heterozygous pathogenic variants in *CHD7*, the gene encoding Chromodomain DNA-binding Protein 7 (CHD7), a chromatin remodeler important for the development of neurons and glial cells. Previous studies in $Chd7^{Gt/+}$ mouse model of CHARGE syndrome showed substantial neuron loss in the early stages of the developing inner ear that are compensated for by mid-gestation. In this study, we sought to determine if early developmental delays caused by *Chd7* haploinsufficiency affect neurons, glial cells, and inner hair cell innervation in the mature cochlea. Analysis of auditory brainstem response recordings in $Chd7^{Gt/+}$ adult animals showed elevated thresholds at 4 kHz and 16 kHz, but no differences in ABR Wave I peak latency or amplitude compared to wild type controls. Proportions of neurons in the $Chd7^{Gt/+}$ adult spiral ganglion and densities of nerve projections from the spiral ganglion to the organ of Corti were not significantly different from wild type controls. Inner hair cell synapse formation also appeared unaffected in mature $Chd7^{Gt/+}$ cochleae. However, histological analysis of adult $Chd7^{Gt/+}$ cochleae revealed diminished satellite glial cells and hypermyelinated Type I spiral ganglion axons. We characterized the expression of CHD7 in developing inner ear glia and found CHD7 to be expressed during a tight window of inner ear development at the Schwann cell precursor stage at E9.5. While cochlear neurons appear to differentiate normally in the setting of *Chd7* haploinsufficiency, our results suggest an important role for CHD7 in glial cells in the inner ear. This study highlights the dynamic nature of CHD7 activity during inner ear development in mice and contributes to understanding CHARGE syndrome pathology.

Keywords

hearing; satellite glial cell; Schwann cell; myelin; ABR; CHARGE syndrome

*Corresponding author: donnamm@med.umich.edu.

1. Introduction

CHARGE syndrome (Coloboma of the eye, Heart defects, Atresia of the choanae, Retardation of growth, Genital hypoplasia, Ear abnormalities) is a developmental disorder occurring in approximately 1 in 10,000 live births annually (Van Ravenswaaij-Arts and Martin, 2017). Ear abnormalities, including mixed conductive/sensorineural hearing loss, are the most penetrant phenotypes in CHARGE (Hale et al., 2016; Van Ravenswaaij-Arts and Martin, 2017). Individuals with CHARGE achieve varying degrees of hearing restoration and improved language from cochlear implants, but abnormalities in temporal bone structure and facial nerve obstruction can disrupt successful implantation of cochlear prosthetics (Choo et al., 2017). Alternative approaches for restoring hearing in CHARGE, such as gene therapy, could significantly benefit from improved understanding of the etiology of sensorineural hearing loss (Hastings and Brigande, 2020; Omichi et al., 2019).

CHARGE syndrome is predominantly caused by pathogenic variants in *CHD7* (*Chd7* in mice), the gene encoding CHD7, a chromatin remodeling enzyme critical for neural development (Bergman et al., 2011; Feng et al., 2017; Van Ravenswaaij-Arts and Martin, 2017; Yao et al., 2020). We have previously demonstrated that the $Chd7^{Gt/+}$ haploinsufficiency mouse model of CHARGE syndrome recapitulates many of the hallmark features of CHARGE, including hearing loss (Adams et al., 2007; Hurd et al., 2011; Layman et al., 2011). Developmental studies of $Chd7^{Gt/+}$ embryos have revealed altered progression of cochleovestibular ganglion (CVG) neurogenesis, in which the population of the CVG by neuroblasts is delayed by 1–2 days of development (Hurd et al., 2010). Whether these defects in neurogenesis have lasting effects through adulthood, or underly the hearing loss observed in $Chd7^{Gt/+}$ mice, has not been determined.

In this study, we sought to address the etiology of hearing loss in $Chd7^{Gt/+}$ adult mice by interrogating multiple components of the peripheral auditory nervous system within the inner ear. Using physiological and histological techniques, we identified a requirement for CHD7 in the development and/or maintenance of satellite glia and myelination of Type I spiral ganglion axons in the adult mouse cochlea. We discovered that while some aspects of cochlear innervation are insensitive to *Chd7* haploinsufficiency, glial cells in the spiral ganglion are uniquely sensitive to *Chd7* loss and may contribute to hearing loss in CHARGE syndrome.

2. Materials & Methods

2.1 Animals

$Chd7^{Gt/+}$ mice were generated as previously described (Hurd et al., 2007) and maintained on a mixed 129S1/Sv1mJ background (The Jackson Laboratory, Stock #002448). Genotyping for the mutant allele was conducted as previously described (Hurd et al., 2010).

Sox10-H2BVenus (Tg(*Sox10-HIST2H2BE/YFP**)^{1Sout}) mice were generated as previously described (Corpening et al., 2011) and maintained on a C3HeB/FeJ background (The Jackson Laboratory, Stock #000658). Genotyping for the intact BAC harboring *Sox10*

regulatory elements and the H2BVenus transgene was conducted as previously described (Corpening et al., 2011).

Animals were housed in a climate-controlled facility on a 12-hour light cycle and provided with food and water *ad libitum.* Mice were euthanized via cervical dislocation followed by decapitation. All procedures involving animals were conducted using protocols approved by the Institutional Animal Care and Use Committee (IACUC) at the University of Michigan and in accordance with the Guide for the Care and Use of Laboratory Animals.

2.2 Auditory Brainstem Response (ABR)

Wild type and *Chd7*$^{Gt/+}$ animals ages 6–8 weeks (N=11, with 5 males and 6 females, in each genotype group) were anesthetized with ketamine (65 mg/kg) and xylazine (3.5 mg/kg) with additional anesthetic administered as needed to maintain anesthesia depth sufficient to insure immobilization and relaxation. Body temperature was maintained with water circulating heating pads and heat lamps. ABRs were recorded in an electrically and acoustically shielded chamber (Acoustic Systems, Austin, TX). Needle electrodes were placed at the vertex (active), the test ear (reference) and the contralateral ear (ground) pinnae. Tucker Davis Technologies (TDT) System III hardware and SigGen/BioSig software (TDT, Alachua, FL) were used for stimulus presentation and response recording. Tones were delivered through an EC1 sound driver (TDT, calibrated in a closed volume approximating the volume of a subject's ear canal with a B&K 1/8 inch microphone), with the speculum consistently placed just inside the tragus. Stimulus presentation consisted of 15 ms tone bursts, with 1 ms rise/fall times, presented at a rate of 10 per second. Up to 1024 responses were averaged for each stimulus level. Responses were collected for stimulus levels 10 dB steps at higher stimulus levels, then with additional 5 dB steps near threshold. Thresholds were interpolated between the lowest stimulus level where a response was observed, and 5 dB lower, where no response was observed. Stimuli were presented at 4, 16, and 32 kHz frequencies for each animal. Two-way ANOVA was conducted to statistically determine the effect of stimulus frequency and/or genotype on ABR thresholds.

ABR waveforms were analyzed in BioSig software. Peaks of Waves I-V were called by two independent observers blinded to genotype of the subjects. Wave I peak latency was defined as the time in milliseconds from stimulus onset to the crest of Wave I. Wave I peak amplitude in nanovolts was defined as the difference in voltage between the crest of Wave I and the preceding trough. Two-way ANOVA was used to statistically determine the effect of stimulus intensity and/or genotype on Wave I peak latency and amplitude.

2.3 Embryo and Inner Ear Collection

To collect *Sox10*-H2BVenus embryos, timed pregnancies were established between *Sox10*-H2BVenus males and wild type females with the morning of seminal plug detection designated as E0.5. Embryos at stages E9.5, E10.5, E14.5, and E17.5 were harvested in cold PBS and fixed in freshly prepared 4% paraformaldehyde (PFA) for 1 hour at room temperature for E10.5 or overnight at 4°C for older embryos. Inner ears were collected from adult wild type and *Chd7*$^{Gt/+}$ animals that were transcardially perfused with freshly prepared 4% PFA. Further fixation of the inner ear was achieved by making a small perforation in the

otic capsule at the apex of the cochlea and slowly perfusing 1mL PFA followed by one hour of fixation at room temperature. Inner ears were processed for whole mount Xgal staining as described previously (Hurd et al., 2011). Samples were infiltrated with 30% sucrose as a cryoprotectant prior to embedding in OCT freezing medium and cryostat sectioning at 12 microns. Frozen sections were stored at −80°C before processing for immunohistochemistry.

2.4 Immunohistochemistry on Frozen Sections

Frozen sections were processed for immunohistochemistry as previously described (Hurd et al., 2010). Briefly, sections were thawed at room temperature, permeabilized in PBS-Tween20, and blocked for one hour in blocking solution. Tissues were incubated overnight at 4°C in primary antibody. For fluorescent staining, sections were incubated in secondary antibody for either direct detection or by Tyramide SuperBoost amplification (TSA, Invitrogen #B40933). Slides were mounted, cover-slipped, and imaged on a Leica DM5000B stereomicroscope. Reagents are all listed in Supplementary Table 1. A minimum of three sections cut from three embryos in each developmental age group were stained for gene expression analysis.

2.5 Immunohistochemistry on Cochlear Whole Mount Preparations and Quantification of Synaptic Puncta

Immunohistochemistry for synaptic markers was conducted in whole mount on cochleae dissected from postnatal mice, using methods described previously (Kurioka et al., 2016; Lee et al., 2016). *Chd7*$^{+/+}$ and *Chd7*$^{Gt/+}$ mice (N=6 per genotype group) were sacrificed at postnatal day 28 (P28) and their temporal bones were collected. Samples were fixed in 4% paraformaldehyde for 1.5 hours and then rinsed with PBS. Epithelia from the apical cochlear region were sub-dissected for processing. Tissues were blocked in 5% Normal Goat Serum and 0.3% Triton X-100 for 1 hour at room temperature and then incubated in primary antibodies against CtBP2 and GluA2 overnight at 4°C. After rinsing with PBS, tissues were incubated in secondary antibodies diluted in 1% Normal Goat Serum for 1 hour at room temperature. Additional rinses with PBS were followed by a final incubation in Phalloidin conjugated to AlexaFluor 488 for 40 minutes. Tissues were rinsed and mounted onto slides with Prolong Gold Anti-Fade mounting media (Invitrogen #P36930). All reagents used are listed in Supplementary Table 1.

Imaging was performed on a Leica Inverted SP5 confocal microscope at the Microscopy & Image Analysis Laboratory at the Biomedical Research Core Facility at the University of Michigan. Z-series confocal stacks were obtained and analyzed in ImageJ software (Schneider et al., 2012). CtBP2/GluA2 positive puncta were marked and counted in each Z-series slice. The total number of double-positive puncta were divided by the number of inner hair cells to obtain average puncta per inner hair cell. Five cochleae were analyzed per genotype. Averages were statistically compared using Student's t-test with significance defined as $p < 0.05$.

2.6 Transmission Electron Microscopy (TEM)

Adult wild type (N=6 male) and *Chd7*$^{Gt/+}$ (N=7 male) mice were transcardially perfused as described above with 2% Glutaraldehyde, 0.15M Cacodylate fixative. Cochleae were

then harvested and perfused with the same fixative, then drop-fixed for a minimum of two hours at room temperature. Cochleae were then placed in 3% EDTA with glutaraldehyde for 10–14 days at room temperature until the bone became soft, with fresh solution replaced every other day. Tissues were then rinsed in cacodylate buffer for ten minutes, incubated in 1% OsO_4 for one hour while shaking, followed by rinsing in water. The cochleae were then incubated in uranyl acetate for 30 minutes while protected from light and thoroughly rinsed in water before proceeding through an alcohol dehydration series. Samples were then washed in propylene oxide and gradually transitioned to Epon embedding media over several hours. Cochleae were embedded in Epon and sectioned through the midmodiolar plane on a Leica Ultracut R ultramicrotome at 80nm thickness and mounted on grids for TEM imaging. Imaging was conducted on a JEM-1400Plus transmission electron microscope (JEOL, Tokyo, Japan) with 80 kV accelerating voltage at 2,500X magnification. The cochlear region of each image (apex vs. base) was noted at the time of imaging.

2.7 G-ratio Analysis

G-ratios from TEM images were measured using a G-ratio calculator plugin for ImageJ (Goebbels et al., 2010) from a minimum of 100 nerves from each cochlea in both apex and base (N=6 male wild type, 7 male $Chd7^{Gt/+}$)). Linear regression analysis was performed to compare G-ratios against axon diameter. Two-way ANOVA tests were used to determine the effect of either region and/or genotype on mean G-ratio, mean myelin thickness, and mean axon diameter between. Statistical effect size was determined by calculating Cohen's *d* coefficient (Lakens, 2013).

2.8 Neuron, Glial Cell, and Axon Projection Counting

Cochleae processed for TEM imaging described above were also used for quantification of spiral ganglion neurons and glial cells. Semi-thin sections in the midmodiolar plane were cut on an ultramicrotome and mounted on slides. The number of spiral ganglion neurons and glial cells were counted in the apex and base regions of the spiral ganglion using previously published methods (Fukui et al., 2012; Kommareddi et al., 2015; Sha et al., 2008). Within the total glial cell group, satellite cells encasing neuron cell bodies and myelinating Schwann cells encasing nerve fibers were quantified. Raw cell counts, as well as spiral ganglion cell density (cells/10,000um^2) were measured in ImageJ. Spiral ganglion area was demarcated by the osseous spiral lamina. A minimum of five sections were quantified for each region of each animal (N=4 wild type males, 6 $Chd7^{Gt/+}$ males). Cell counts were conducted by two independent observers blinded to animal genotypes. The statistical effect of cochlear region (apex vs. base) and genotype (wild type vs. $Chd7^{Gt/+}$) was tested via two-way ANOVA with Tukey's HSD post-hoc test. Statistical effect size was determined by Cohen's *d* coefficient (Lakens, 2013). This same procedure was used to determine the density of axon projections from the spiral ganglion to the organ of Corti.

3. Results

3.1 *Chd7*$^{Gt/+}$ mice exhibit low frequency-specific hearing loss but normal Wave I latency and amplitude

In a previous study of adult *Chd7*$^{Gt/+}$ mice, we reported elevated thresholds of air-conduction ABR at 4 and 16 kHz stimulus frequencies (Hurd et al., 2011). Here we asked whether additional deficits in auditory signal propagation could be detected by ABR. From a new cohort of wild type and *Chd7*$^{Gt/+}$ male and female mice (N=11 in each genotype group), we recorded ABRs at 4, 16, and 32 kHz frequencies. In addition to measuring ABR threshold, we collected two additional data points: Wave I peak amplitude, an indicator of auditory nerve signal propagation strength, and Wave I peak latency, an indicator of speed of neurotransmission through the auditory nerve (Fig 1A). As previously reported, we found that adult *Chd7*$^{Gt/+}$ mice exhibit significantly increased ABR thresholds at 4 kHz (39 dB SPL vs 80 dB SPL, $p = 7.11^{-6}$) and 16 kHz (22 dB SPL vs 47 dB SPL, $p = 0.00105$) stimulus frequencies, but not at 32 kHz (51 dB SPL vs 49 dB SPL, $p = 0.88$) (Fig 1B). We computed and examined average ABR waveforms for each stimulus frequency and noted that *Chd7*$^{Gt/+}$ waveforms do not appear different from those of wild type littermate controls (Fig 1C, F, I). We calculated and compared input/output (I/O) growth functions for Wave I peak latency (Fig 1D, G, J) and for Wave I peak amplitude (Fig 1E, H, K), and found no statistically significant differences in either of these measures of auditory nerve function between *Chd7*$^{Gt/+}$ and wild type littermate controls. These experimental results suggest that auditory nerve function is normal in *Chd7*$^{Gt/+}$ mice or that such deficiencies are present but below the level of detection using air conduction ABR. To help explore these possibilities, we carefully examined the cochlear spiral ganglion, organ of Corti, and auditory nerve in *Chd7*$^{Gt/+}$ mutant mice.

3.2 Neuron densities are normal but satellite glial cells are reduced in adult *Chd7*$^{Gt/+}$ spiral ganglion

Previous studies of embryonic development in *Chd7*$^{Gt/+}$ mice demonstrated a developmental delay during embryogenesis in the production of cells in the cochleovestibular ganglion (CVG) (Hurd et al., 2010). *Chd7*$^{Gt/+}$ embryos exhibit substantially fewer neuroblasts in the CVG at E10.5, but cell numbers recovered to wild type levels by E11.5 (Hurd et al., 2010). However, whether this delay in CVG cell production affects neurons and glial cells in similar proportions in the adult spiral ganglion is unknown. To answer this question, we examined mid-modiolar plane sections of the apex, middle, and base regions of the cochlea in 8-week-old wild type (N=4) and *Chd7*$^{Gt/+}$ (N=6) male animals and measured spiral ganglion neuron and glial cell density (Fig 2). We observed no morphological abnormalities of the spiral ganglion in *Chd7*$^{Gt/+}$ cochleae (Fig 2A–D). We measured the density of neurons in the spiral ganglia and found the mean apex neuron densities were 9.76 ± 0.83 neurons/10 mm^2 in wild type, versus 8.91 ± 0.59 neurons/10 mm^2 in *Chd7*$^{Gt/+}$ spiral ganglia. Average base neuron densities were 9.72 ± 0.36 neurons/10 mm^2 in wild type ears spiral ganglia, versus 9.39 ± 0.25 neurons/10 mm^2 in *Chd7*$^{Gt/+}$ samples (Fig 2E). We used two-way ANOVA with Tukey's HSD post-hoc test to determine if region of the cochlea or genotype affected cell density in the spiral ganglion. There were no statistically significant differences

in average neuron density by region (f(1) = 0.305, p = 0.5877) or genotype (f(1) = 1.284, p = 0.2729).

We also measured the density of glial cells in the spiral ganglion in wild type and *Chd7*$^{Gt/+}$ cochleae. In our analyses, we separately counted two glial cell populations in the cochlea: satellite glial cells that provide neurotrophic support to spiral ganglion neuronal cell bodies, and myelinating Schwann cells that encase peripheral nerve projections from the spiral ganglion to the organ of Corti (Lago-Baldaia et al., 2020). Our measurements showed a significant reduction in satellite glial cells in *Chd7*$^{Gt/+}$ cochleae (f(1)=5.103, p=0.373, two-way ANOVA), with no effect of region (f(1)=0.026, p=0.875, two-way ANOVA) (Fig 2F). Apex satellite glial cell densities were 4.37 ± 0.49 glial cells/10mm^2 in wild type spiral ganglia, compared to 3.36 ± 0.16 glial cells/10 mm^2 in *Chd7*$^{Gt/+}$ samples. The difference in apex satellite glial cell densities exhibited a large statistical effect size (Cohen's *d*=1.496). In the base, mean satellite glial cell densities were measured as 4.22 ± 0.72 cells/10 mm^2 in wild type vs. 3.56 ± 0.19 cells/10 mm^2, with a moderate effect size (Cohen's *d*=0.686).. Interestingly, myelinating Schwann cell densities tended to be reduced in *Chd7*$^{Gt/+}$ cochleae, but cell density differences between genotypes narrowly missed statistical significance (f(1)=4.171, p=0.058, two-way ANOVA) (Fig 2G). Cochlear region did not impact differences in Schwann cell densities between genotypes (f(1)=0.149, p=0.704). Mean apex Schwann cell densities were measured as 8.652 ± 1.48 cells/10mm^2 in wild type and 7.768 ± 0.515 in *Chd7*$^{Gt/+}$ ears respectively. Mean base Schwann cell densities were similar to apex measurements; 9.013 ± 0.314 cells/10mm^2 in wild type vs. 7.026 ± 0.361 cells/10mm^2 in *Chd7*$^{Gt/+}$ samples. From this experiment, we conclude that glial cells are specifically affected by loss of *Chd7*, while spiral ganglion neurons are insensitive to *Chd7* haploinsufficiency.

3.3 *Chd7* haploinsufficiency does not impact the density of spiral ganglion afferent projections

Although proportions of neurons were unaffected by *Chd7* loss, we next questioned if CHD7 is required for the outgrowth of nerve fibers projecting from the spiral ganglion to the organ of Corti by measuring the density of myelinated axons traversing through the osseous spiral lamina in the apex and base of the cochlea in wild type (N=8 male) and *Chd7*$^{Gt/+}$ (N=8 male) 8-week old mice (Fig 3). The overall morphology of the nerve bundles in Rosenthal's canal appeared comparable between wild type and *Chd7*$^{Gt/+}$ cochleae imaged by TEM (Fig 3A). Average apex nerve densities in wild type and *Chd7*$^{Gt/+}$ samples were not statistically significantly different (9.7 neurons/10 mm^2 vs. 8.9 neurons/10 mm^2), nor were average nerve densities in the base (7.21 ± 0.77 nerves/100 μm^2 in wild type vs. 8.09 ± 1.21 nerves/100 μm^2 in *Chd7*$^{Gt/+}$) (Fig 3B). Two-way ANOVA showed no effect of cochlear region on axon density (f(1) = 2.967, p = 0.096) nor genotype (f(1) = 0.004, p = 0.947). These experimental results indicate that loss of one copy of *Chd7* does not alter the ability of Type I spiral ganglion neurons to traverse the osseous spiral lamina and project to the organ of Corti.

3.4 Loss of *Chd7* does not affect formation of inner hair cell synaptic terminals

Formation of intact synapses from Type I spiral ganglion neurons on inner hair cells (IHC) in the organ of Corti is critical for inner ear development. We investigated if *Chd7* is required for this developmental process by quantifying synaptic puncta in P28 wild type and $Chd7^{Gt/+}$ cochleae (Fig 4, N=6 male animals per genotype group). Whole mount apical cochlear preparations were stained with CtBP2 (presynaptic marker) and GluA2 (postsynaptic marker) and imaged via confocal microscopy. Samples were counter-stained with phalloidin to visualize hair cells and the average number of intact synaptic puncta, defined as overlap of CtBP2 and GluA2, were measured in wild type (Fig 4A–A") and $Chd7^{Gt/+}$ animals (Fig 4B–B"). We found no statistically significant difference in the average number of intact synaptic puncta between the two genotype groups (12.82 ± 0.86 puncta/IHC in wild type vs. 13.76 ± 1.01 puncta/IHC in $Chd7^{Gt/+}$, p = 0.4952, Welch's t-test, Fig 4C). This result suggests that CHD7 is not required for the formation of inner hair cell synapses in the auditory sensory epithelium.

3.5 *Chd7* is required for appropriate myelination of Type I neurons in the spiral ganglion

Previous studies in a mouse model of CHARGE syndrome revealed a critical role for CHD7 in regulating myelination in the central nervous system (CNS) (He et al., 2016). We hypothesized that CHD7 may similarly regulate myelination in the peripheral auditory nervous system. To test this, we processed 8-week-old wild type (N=6 male) and $Chd7^{Gt/+}$ (N=7 male) cochleae for TEM and quantified myelination of spiral ganglion neurons (Fig 5). We noted an increase in myelin thickness in $Chd7^{Gt/+}$ cochleae compared to wild type littermates (Fig 5A). The overall G-ratio throughout the entire cochlea was significantly decreased in $Chd7^{Gt/+}$ mutant spiral ganglia compared to wild type (0.707 ± 0.004 in wild type vs. 0.671 ± 0.006 in $Chd7^{Gt/+}$, p = 0.001015, Welch's t-test, Fig 5B). While the decrease in $Chd7^{Gt/+}$ G-ratio is subtle, it is of large statistical effect size (Cohen's d=2.46). Both wild type and $Chd7^{Gt/+}$ spiral ganglion nerves showed a linear relationship between axon diameter and G-ratio in the apex and base of the cochlea, indicating that nerve fibers of all sizes exhibited altered myelination through the entire length of the cochlea (Fig 5C–D). To determine if myelin thickness was driving the lower average G-ratio in $Chd7^{Gt/+}$ samples, we separated the myelin thickness and axon diameter measurements from the G-ratios and analyzed them individually in both apex and base regions. Indeed, myelin thickness increased by 10% in the apex and 15% in base $Chd7^{Gt/+}$ spiral ganglia compared to wild type samples (0.5704 ± 0.0028 μm vs. 0.6284 ± 0.0042 μm in apex, 0.5782 ± 0.0032 μm vs. 0.6702 ± 0.0038 μm in base, f(1)=7.542, p=0.0128, two-way ANOVA) (Fig 5E–F). However, mean axon diameter was not significantly different between the two genotype groups in either apex or base regions (1.422 ± 0.0061 μm in wild type vs. 1.428 ± 0.0077 μm in $Chd7^{Gt/+}$ apex spiral ganglia, and 1.351 ± 0.0069 μm vs 1.308 ± 0.0059 μm in wild type and $Chd7^{Gt/+}$ base spiral ganglia respectively, f(1)=0.070, p = 0.795, two-way ANOVA, Fig 5G–H). From these results, we conclude that CHD7 participates in the regulation of myelination of Type I spiral ganglion neurons.

3.6 *Chd7* is expressed in migratory neural crest and Schwann cell precursors populating the cochleovestibular ganglion

Chd7 is known to be expressed in developing CVG neurons (Hurd et al., 2010), but its expression in developing glia has not been characterized. We employed a transgenic *Sox10*-h2BVenus mouse line that faithfully recapitulates endogenous expression of *Sox10*, a transcription factor expression in neural crest cells fated to become Schwann cells and satellite glial cells (Corpening et al., 2011; Jessen et al., 2015). We collected *Sox10*-h2BVenus transgenic embryos at stages E9.5, E10.5, E14.5, and E17.5 and stained transverse cryo-sections with anti-CHD7 antibody (Fig 6, N=at least 3 sections from 3 embryos per age group). At stage E9.5, neural crest cells rostral to the otocyst are emigrating ventrally from the neural tube, some which express *Sox10*-H2BVenus (Fig 6A) or CHD7 (Fig 6B). We noted some co-localization between *Sox10*-H2BVenus and CHD7 in this cell population (Fig 6C), which corroborates previous reports of *Chd7* expression in neural crest cell lineages (Bajpai et al., 2010; Fan et al., 2021; Fujita et al., 2016). Examination of the CVG at E9.5, which ultimately gives rise to the cochlear spiral ganglion and vestibular ganglion (Coate and Kelley, 2013), showed extensive expression of CHD7 in *Sox10*-H2BVenus+ Schwann cell precursors (Fig 6B–B”). A similar pattern of expression was also present in the caudal CVG, although with more CHD7+,*Sox10*-H2BVenus- cells that are likely neuronal in identity (Fig 6C–C”). Interestingly, by one day later at E10.5, CHD7 was largely excluded from *Sox10*-H2BVenus+ cells in the CVG (Fig 6D–D”). By E14.5, CHD7 and *Sox10*-H2BVenus expression were mutually exclusive in the spiral ganglion (Fig 6E–E”) and this expression pattern continued through E17.5 (Fig 6F–F”). From this gene expression analysis, we conclude that CHD7 is initially robustly expressed in neural crest-derived Schwann cell precursors during the earliest stages of CVG formation but is rapidly down-regulated in developing glial cells at E10.5.

4. Discussion

In this study, we sought to determine the etiology of hearing loss observed in the $Chd7^{Gt/+}$ mouse model of CHARGE syndrome. By systematically investigating the core components of the peripheral auditory system, we found that cochlear innervation is preserved with loss of one copy of *Chd7*. Interestingly, we discovered a novel function for CHD7 in the development and/or maintenance of satellite glial cells in the spiral ganglia and in regulating myelin sheaths encasing Type I spiral ganglion neurons innervating the auditory sensory epithelium of the cochlea. These findings have important implications for CHD7 function in the peripheral nervous system and CHARGE syndrome.

This study builds upon previous work showing hearing loss at low- and mid-range frequencies in $Chd7^{Gt/+}$ mice but not higher frequencies (Hurd et al., 2011). Here we also found normal Wave I peak latencies and amplitudes, wild type proportions of spiral ganglion neurons, neuronal projections, and IHC synapses in $Chd7^{Gt/+}$ cochleae. These observations together suggest that the auditory nerve is normal and functional in this model of CHARGE syndrome. It is possible that other chromatin remodelers may be able to act in a compensatory manner to mitigate loss of *Chd7*. CHD7 functions as part of a large protein complex that includes other chromatin remodelers, such as BRG1 (Bajpai et al.,

2010; Martin, 2010). Future experiments will investigate whether CHD7-interacting partners like BRG1 are up-regulated in *Chd7*$^{Gt/+}$ tissues.

Using the *Chd7*$^{Gt/+}$ mouse line, our group also previously demonstrated a delay at E10.5 in the delamination of neuroblasts from the otocyst that give rise to the CVG. Neuroblasts in *Chd7*$^{Gt/+}$ mice are normal by E11.5 (Hurd et al., 2010). Normal numbers of neurons in the *Chd7*$^{Gt/+}$ CVG suggests that this initial delay in neuroblast production in the CVG does not impact neuron numbers in the adult spiral ganglion. Recent studies characterizing the genetic diversity of spiral ganglion neurons have also demonstrated at least four neuronal subtypes in the ganglion: Type 1a, 1b, 1c, and Type 2 (Shrestha et al., 2018; Sun et al., 2018). It will be interesting to determine how early these neuronal subtypes are specified in development and whether these subtypes are disrupted in *Chd7*$^{Gt/+}$ mice.

In this study, we observed a significant reduction in the density of satellite glial cells within the spiral ganglion of *Chd7*$^{Gt/+}$ cochleae. Satellite glial cells provide important neurotrophic support to neurons within the spiral ganglia and other peripheral sensory and motor systems (Lago-Baldaia et al., 2020). A prior study reported spiral ganglion neuronal degeneration upon loss of satellite glial cells in mice, which led to subsequent hearing loss (Akil et al., 2015). In our study, we did not find evidence of neuronal degeneration in *Chd7*$^{Gt/+}$ spiral ganglia, but it is possible that a deficit in satellite glia could alter neuronal physiology in the cochlea that could contribute, at least in part, to hearing loss. In addition to reduced satellite glial cells, we observed a subtle but significant increase in myelination of *Chd7*$^{Gt/+}$ spiral ganglion nerve projections to the organ of Corti. Aberrant myelination of spiral ganglion neurons can have a significant impact on the function of the auditory nerve and hearing. Deafness in peripheral neuropathies, such as Charcot-Marie-Tooth syndrome, as well as Hidden Hearing Loss, can be attributed (at least in part) to defective myelination of spiral ganglion neurons (Long et al., 2018; Wan and Corfas, 2017). Indeed, one of the causative genes of Charcot-Marie-Tooth, *Pmp22*, encodes a core myelin component and loss of function of *Pmp22* in mice leads to both hypermyelination and demyelination of peripheral nerves (Adlkofer et al., 1995; Bolino et al., 2016; Sander et al., 1998). CHD7 may be an upstream regulator of *Pmp22* or other essential myelination genes, such as *Mpz,* or *Plp1* (Kastriti and Adameyko, 2017). We were surprised to note that, despite observing a significant increase in myelin sheath thickness in *Chd7*$^{Gt/+}$ cochleae, there was no statistically significant difference in Wave I peak latency in ABR recordings. It is important to note that even a small alteration in myelination can significantly impact nerve conduction velocity, but ABR is not the most sensitive means to determine if this is the case. Future studies will investigate this question using *in vivo* electrophysiological recording of nerve conduction velocity (Schulz et al., 2014).

CHD7 has been the subject of numerous studies focused on CNS development, including neurons and oligodendrocytes (Feng et al., 2017; He et al., 2016; Reddy et al., 2021). Despite the numerous peripheral nervous system (PNS) related clinical features of CHARGE, the PNS has not been as thoroughly studied in CHD7 animal models. The current report is an important contribution to the study of peripheral phenotypes of CHARGE syndrome. Other studies have illustrated the importance of CHD7 in early neural crest developmental events, including neural crest specification, neural crest stem cell formation,

and the development of craniofacial mesenchyme (Bajpai et al., 2010; Fan et al., 2021; Fujita et al., 2016). To our knowledge, this is the first report of a role for CHD7 in the development and/or maintenance of satellite glia and, as well as the production of myelin in Schwann cells. In this study, we found that CHD7 is indeed expressed in early-stage neural crest-derived Schwann cell precursors (SCPs) that give rise to both satellite glia and myelinating Schwann cells (Kastriti and Adameyko, 2017).. In embryonic development, the SCP population bifurcates into two genetically distinct glial cell lineages: immature Schwann cells and satellite glial cells. Given our observation that *Chd7* expression is downregulated in glia by E14.5, about the time that immature Schwann cell and satellite glial lineages diverge, it is possible that satellite glia fail to properly develop from the SCP cell state with loss of *Chd7*. Another possibility is that the cell loss and increased myelin production we observed in $Chd7^{Gt/+}$ mice is a non-cell autonomous effect of *Chd7* loss in spiral ganglion neurons (Jessen et al., 2015; Long et al., 2018). Non-cell autonomous functions of CHD7 could also play a role in neuron-glia interactions between spiral ganglion neurons and satellite glia (Lago-Baldaia et al., 2020); a disruption in cell-cell communication mechanisms could lead to aberrant development or death of satellite glia. For example, Neuregulin-ErbB receptor signaling between neurons and Schwann cells plays a critical role in regulating myelin production through development and adulthood (Birchmeier and Nave, 2008; Brinkmann et al., 2008; Chen et al., 2006). It is possible that CHD7 regulates the expression of Neuregulin in spiral ganglion neurons. Future studies will investigate neuron-glia interactions in the developing inner ear.

It is important to note that $Chd7^{Gt/+}$ mice also exhibit middle ear defects, including stapedial malformations that result in ossicular chain fixation and ankylosis (Hurd et al., 2011). Given the lack of overt neural inner ear phenotypes, it is possible that the increased ABR thresholds observed in $Chd7^{Gt/+}$ mice are indicative of primarily conductive hearing loss, rather than sensorineural. Air conduction ABR relies on the presentation of sound stimuli through the external ear canal and the middle ear, which presents a confounding variable in analysis of hearing in $Chd7^{Gt/+}$ mice. Overall, this work demonstrates that in the mouse, cochlear innervation is insensitive to *Chd7* haploinsufficiency, with the exception of glial cells and myelination in the spiral ganglia. We have demonstrated a previously unknown role for CHD7 in myelin production in the peripheral nervous system that informs our understanding of inner ear pathology in CHARGE syndrome and CHD7-related disorders.

Supplementary Material

Refer to Web version on PubMed Central for supplementary material.

Acknowledgements

TEM was conducted in the Microscopy and Imaging Laboratory in the Biomedical Research Core Facility at the University of Michigan, which is supported by NIH grant P30-CA046592. We thank Sasha Meshinchi for his help and advice in TEM imaging. We also thank Jennifer Skidmore for mouse colony management, and members of the Martin and Raphael laboratories for insightful comments and support. This work was supported by grants NIH R01-DC014456 (DMM and YR), NIH R01-DC018404 (DMM), the University of Michigan Taubman Scholars Award (DMM), and the R. Jamison and Betty Williams Professorship (YR). KER was supported by NIH T32-DC000011.

References

Adams ME, Hurd EA, Beyer LA, Swiderski DL, Raphael Y, Martin DM, 2007. Defects in vestibular sensory epithelia and innervation in mice with loss of Chd7 function: implications for human CHARGE syndrome. J Comp Neurol 504, 519–532. [PubMed: 17701983]

Adlkofer K, Martini R, Aguzzi A, Zielasek J, Toyka KV, Suter U, 1995. Hypermyelination and demyelinating peripheral neuropathy in Pmp22-deficient mice. Nat Genet 11, 274–280. [PubMed: 7581450]

Akil O, Sun Y, Vijayakumar S, Zhang W, Ku T, Lee CK, Jones S, Grabowski GA, Lustig LR, 2015. Spiral ganglion degeneration and hearing loss as a consequence of satellite cell death in saposin B-deficient mice. J Neurosci 35, 3263–3275. [PubMed: 25698761]

Bajpai R, Chen DA, Rada-Iglesias A, Zhang J, Xiong Y, Helms J, Chang CP, Zhao Y, Swigut T, Wysocka J, 2010. CHD7 cooperates with PBAF to control multipotent neural crest formation. Nature 463, 958–962. [PubMed: 20130577]

Bergman JE, Janssen N, Hoefsloot LH, Jongmans MC, Hofstra RM, Van Ravenswaaij-Arts C, 2011. CHD7 mutations and CHARGE syndrome: the clinical implications of an expanding phenotype. J Med Genet 48, 334–342. [PubMed: 21378379]

Birchmeier C, Nave KA, 2008. Neuregulin-1, a key axonal signal that drives Schwann cell growth and differentiation. Glia 56, 1491–1497. [PubMed: 18803318]

Bolino A, Piguet F, Alberizzi V, Pellegatta M, Rivellini C, Guerrero-Valero M, Noseda R, Brombin C, Nonis A, D'Adamo P, Taveggia C, Previtali SC, 2016. Niacin-mediated Tace activation ameliorates CMT neuropathies with focal hypermyelination. EMBO Mol Med 8, 1438–1454. [PubMed: 27799291]

Brinkmann BG, Agarwal A, Sereda MW, Garratt AN, Muller T, Wende H, Stassart RM, Nawaz S, Humml C, Velanac V, Radyushkin K, Goebbels S, Fischer TM, Franklin RJ, Lai C, Ehrenreich H, Birchmeier C, Schwab MH, Nave KA, 2008. Neuregulin-1/ErbB signaling serves distinct functions in myelination of the peripheral and central nervous system. Neuron 59, 581–595. [PubMed: 18760695]

Chen S, Velardez MO, Warot X, Yu ZX, Miller SJ, Cros D, Corfas G, 2006. Neuregulin 1-erbB signaling is necessary for normal myelination and sensory function. J Neurosci 26, 3079–3086. [PubMed: 16554459]

Choo DI, Tawfik KO, Martin DM, Raphael Y, 2017. Inner ear manifestations in CHARGE: Abnormalities, treatments, animals, models, and progress toward treatments in auditory and vestibular structures. Am J Med Genet C Semin Med Genet 175, 439–449. [PubMed: 29082607]

Coate TM, Kelley MW, 2013. Making connections in the inner ear: recent insights into the development of spiral ganglion neurons and their connectivity with sensory hair cells. Semin Cell Dev Biol 24, 460–469. [PubMed: 23660234]

Corpening JC, Deal KK, Cantrell VA, Skelton SB, Buehler DP, Southard-Smith EM, 2011. Isolation and live imaging of enteric progenitors based on Sox10-Histone2BVenus transgene expression. genesis 49, 599–618. [PubMed: 21504042]

Fan X, Masamsetti VP, Sun JQ, Engholm-Keller K, Osteil P, Studdert J, Graham ME, Fossat N, Tam PP, 2021. TWIST1 and chromatin regulatory proteins interact to guide neural crest cell differentiation. Elife 10.

Feng W, Kawauchi D, Korkel-Qu H, Deng H, Serger E, Sieber L, Lieberman JA, Jimeno-Gonzalez S, Lambo S, Hanna BS, Harim Y, Jansen M, Neuerburg A, Friesen O, Zuckermann M, Rajendran V, Gronych J, Ayrault O, Korshunov A, Jones DT, Kool M, Northcott PA, Lichter P, Cortes-Ledesma F, Pfister SM, Liu HK, 2017. Chd7 is indispensable for mammalian brain development through activation of a neuronal differentiation programme. Nat Commun 8, 14758. [PubMed: 28317875]

Fujita K, Ogawa R, Ito K, 2016. CHD7, Oct3/4, Sox2, and Nanog control FoxD3 expression during mouse neural crest-derived stem cell formation. FEBS J 283, 3791–3806. [PubMed: 27579714]

Fukui H, Wong HT, Beyer LA, Case BG, Swiderski DL, Di Polo A, Ryan AF, Raphael Y, 2012. BDNF gene therapy induces auditory nerve survival and fiber sprouting in deaf Pou4f3 mutant mice. Sci Rep 2, 838. [PubMed: 23150788]

Goebbels S, Oltrogge JH, Kemper R, Heilmann I, Bormuth I, Wolfer S, Wichert SP, Mobius W, Liu X, Lappe-Siefke C, Rossner MJ, Groszer M, Suter U, Frahm J, Boretius S, Nave KA, 2010. Elevated phosphatidylinositol 3,4,5-trisphosphate in glia triggers cell-autonomous membrane wrapping and myelination. J Neurosci 30, 8953–8964. [PubMed: 20592216]

Hale CL, Niederriter AN, Green GE, Martin DM, 2016. Atypical phenotypes associated with pathogenic CHD7 variants and a proposal for broadening CHARGE syndrome clinical diagnostic criteria. Am J Med Genet A 170A, 344–354. [PubMed: 26590800]

Hastings ML, Brigande JV, 2020. Fetal gene therapy and pharmacotherapy to treat congenital hearing loss and vestibular dysfunction. Hear Res 394, 107931. [PubMed: 32173115]

He D, Marie C, Zhao C, Kim B, Wang J, Deng Y, Clavairoly A, Frah M, Wang H, He X, Hmidan H, Jones BV, Witte D, Zalc B, Zhou X, Choo DI, Martin DM, Parras C, Lu QR, 2016. Chd7 Cooperates with Sox10 and Regulates the Onset of CNS Myelination and Remyelination. Nat Neurosci 19, 678–689. [PubMed: 26928066]

Hurd EA, Adams ME, Layman WS, Swiderski DL, Beyer LA, Halsey KE, Benson JM, Gong TW, Dolan DF, Raphael Y, Martin DM, 2011. Mature middle and inner ears express Chd7 and exhibit distinctive pathologies in a mouse model of CHARGE syndrome. Hear Res 282, 184–195. [PubMed: 21875659]

Hurd EA, Capers PL, Blauwkamp MN, Adams ME, Raphael Y, Poucher HK, Martin DM, 2007. Loss of Chd7 function in gene-trapped reporter mice is embryonic lethal and associated with severe defects in multiple developing tissues. Mamm Genome 18, 94–104. [PubMed: 17334657]

Hurd EA, Poucher HK, Cheng K, Raphael Y, Martin DM, 2010. The ATP-dependent chromatin remodeling enzyme CHD7 regulates pro-neural gene expression and neurogenesis in the inner ear. Development 137, 3139–3150. [PubMed: 20736290]

Jessen KR, Mirsky R, Lloyd AC, 2015. Schwann Cells: Development and Role in Nerve Repair. Cold Spring Harb Perspect Biol 7, a020487. [PubMed: 25957303]

Kastriti ME, Adameyko I, 2017. Specification, plasticity and evolutionary origin of peripheral glial cells. Curr Opin Neurobiol 47, 196–202. [PubMed: 29161639]

Kommareddi P, Nair T, Kakaraparthi BN, Galano MM, Miller D, Laczkovich I, Thomas T, Lu L, Rule K, Kabara L, Kanicki A, Hughes ED, Jones JM, Hoenerhoff M, Fisher SG, Altschuler RA, Dolan D, Kohrman DC, Saunders TL, Carey TE, 2015. Hair Cell Loss, Spiral Ganglion Degeneration, and Progressive Sensorineural Hearing Loss in Mice with Targeted Deletion of Slc44a2/Ctl2. J Assoc Res Otolaryngol 16, 695–712. [PubMed: 26463873]

Kurioka T, Lee MY, Heeringa AN, Beyer LA, Swiderski DL, Kanicki AC, Kabara LL, Dolan DF, Shore SE, Raphael Y, 2016. Selective hair cell ablation and noise exposure lead to different patterns of changes in the cochlea and the cochlear nucleus. Neuroscience 332, 242–257. [PubMed: 27403879]

Lago-Baldaia I, Fernandes VM, Ackerman SD, 2020. More Than Mortar: Glia as Architects of Nervous System Development and Disease. Front Cell Dev Biol 8, 611269. [PubMed: 33381506]

Lakens D, 2013. Calculating and reporting effect sizes to facilitate cumulative science: a practical primer for t-tests and ANOVAs. Front Psychol 4, 863. [PubMed: 24324449]

Layman WS, Hurd EA, Martin DM, 2011. Reproductive Dysfunction and Decreased GnRH Neurogenesis in a Mouse Model of CHARGE Syndrome. Hum Mol Genet 20, 3138–3150. [PubMed: 21596839]

Lee MY, Kurioka T, Nelson MM, Prieskorn DM, Swiderski DL, Takada Y, Beyer LA, Raphael Y, 2016. Viral-mediated Ntf3 overexpression disrupts innervation and hearing in nondeafened guinea pig cochleae. Mol Ther Methods Clin Dev 3, 16052. [PubMed: 27525291]

Long P, Wan G, Roberts MT, Corfas G, 2018. Myelin Development, Plasticity, and Pathology in the Auditory System. Dev Neurobiol 78, 80–92. [PubMed: 28925106]

Martin DM, 2010. Chromatin remodeling in development and disease: focus on CHD7. PLoS Genet 6, e1001010. [PubMed: 20657659]

Omichi R, Shibata SB, Morton CC, Smith RJH, 2019. Gene therapy for hearing loss. Hum Mol Genet 28, R65–R79. [PubMed: 31227837]

Reddy NC, Majidi SP, Kong L, Nemera M, Ferguson CJ, Moore M, Goncalves TM, Liu HK, Fitzpatrick JAJ, Zhao G, Yamada T, Bonni A, Gabel HW, 2021. CHARGE syndrome protein

CHD7 regulates epigenomic activation of enhancers in granule cell precursors and gyrification of the cerebellum. Nat Commun 12, 5702. [PubMed: 34588434]

Sander S, Nicholson GA, Ouvrier RA, McLeod JG, Pollard JD, 1998. Charcot-Marie-Tooth disease: histopathological features of the peripheral myelin protein (PMP22) duplication (CMT1A) and connexin32 mutations (CMTX1). Muscle Nerve 21, 217–225. [PubMed: 9466597]

Schneider CA, Rasband WS, Eliceiri KW, 2012. NIH Image to ImageJ: 25 years of image analysis. Nat Methods 9, 671–675. [PubMed: 22930834]

Schulz A, Walther C, Morrison H, Bauer R, 2014. In vivo electrophysiological measurements on mouse sciatic nerves. J Vis Exp.

Sha SH, Kanicki A, Dootz G, Talaska AE, Halsey K, Dolan D, Altschuler R, Schacht J, 2008. Age-related auditory pathology in the CBA/J mouse. Hear Res 243, 87–94. [PubMed: 18573325]

Shrestha BR, Chia C, Wu L, Kujawa SG, Liberman MC, Goodrich LV, 2018. Sensory Neuron Diversity in the Inner Ear is Shaped by Activity. Cell 174, 1229–1246.e1217. [PubMed: 30078709]

Sun S, Babola T, Pregernig G, So KS, Nguyen M, Su S-SM, Palermo AT, Bergles DE, Burns JC, Muller U, 2018. Hair Cell Mechanotransduction Regulates Spontaneous Activity and Spiral Ganglion Subtype Specification in the Auditory System. Cell 174, 1247–1263.e1215. [PubMed: 30078710]

Van Ravenswaaij-Arts C, Martin DM, 2017. New Insights and Advances in CHARGE Syndrome: Diagnosis, Etiologies, Treatments, and Research Discoveries. Am J Med Genet C Semin Med Genet 175, 397–406. [PubMed: 29171162]

Wan G, Corfas G, 2017. Transient auditory nerve demyelination as a new mechanism for hidden hearing loss. Nat Commun 8, 14487. [PubMed: 28211470]

Yao H, Hannum DF, Zhai Y, Hill SF, Albanus RD, Lou W, Skidmore JM, Sanchez G, Saiakhova A, Bielas SL, Scacheri P, Ljungman M, Parker SCJ, Martin DM, 2020. CHD7 promotes neural progenitor differentiation in embryonic stem cells via altered chromatin accessibility and nascent gene expression. Sci Rep 10, 17445. [PubMed: 33060836]

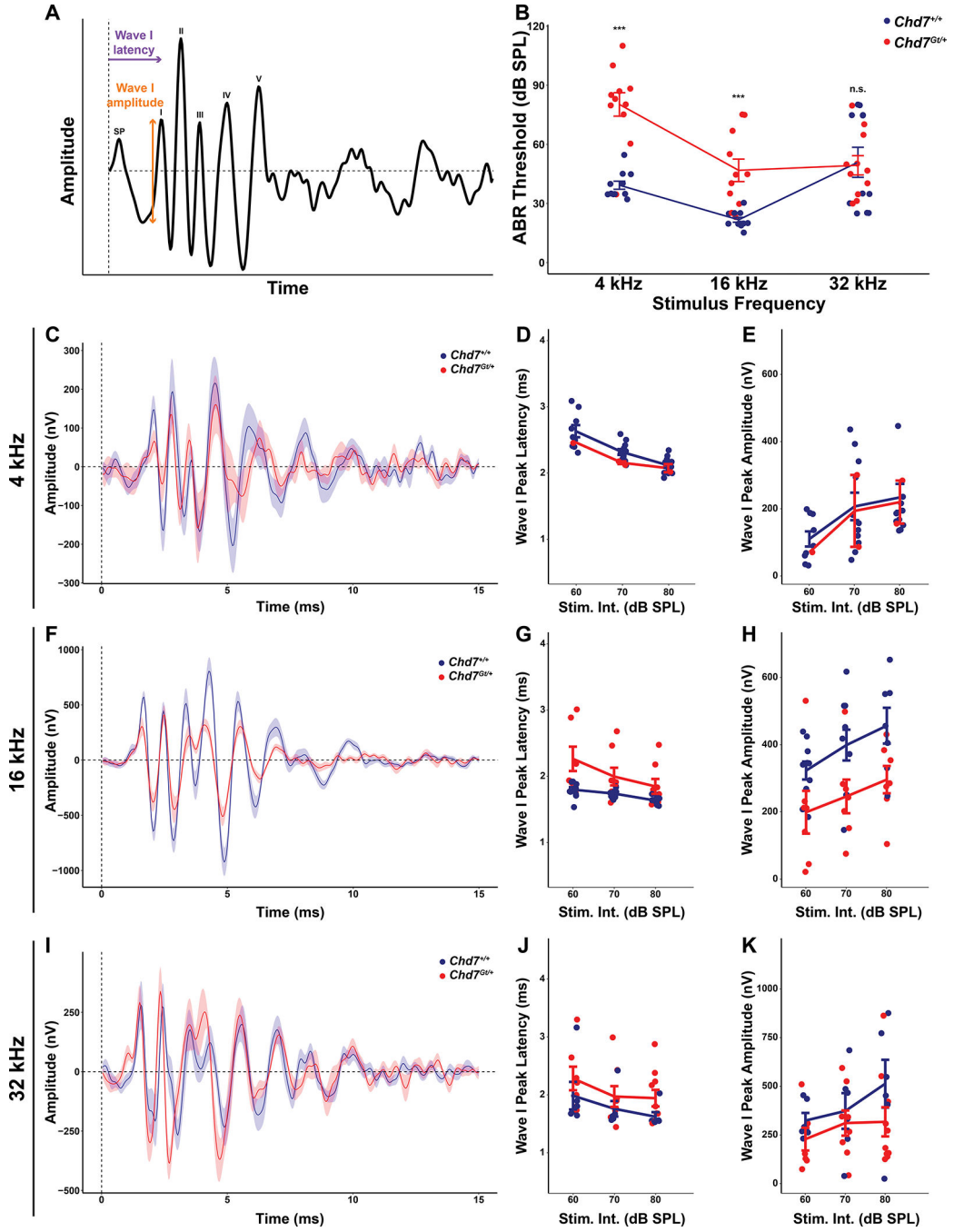

Figure 1. Elevated air-conduction ABR thresholds at low stimulus frequencies but unaltered Wave I peak latency and amplitude in adult *Chd7*$^{Gt/+}$ mice.

(A) Schematic of typical ABR waveform with peaks labeled and Wave I peak latency and amplitude defined. (B) ABR thresholds at 4, 16, and 32 kHz stimulus frequencies in 6 to 8-week-old wild type (blue) and *Chd7*$^{Gt/+}$ (red) male and female mice. N=11 wild type mice (5 male) and 11 *Chd7*$^{Gt/+}$ mice (5 male). *** denotes $p < 0.001$ by two-way ANOVA. (C) Average ABR waveforms (solid line) with standard error of the mean (ribbons) recorded at 4 kHz stimulus frequency in wild type (blue) and *Chd7*$^{Gt/+}$ (red) mice. Vertical and horizontal dashed lines represent stimulus onset and noise floor, respectively. (D) Wave I peak latency

(ms) at 4 kHz stimulus frequency plotted against stimulus intensity (dB SPL). Each dot is one animal. Error bars represent standard error of the mean. (E) Wave I peak amplitude (nV) plotted against stimulus intensity (dB SPL) for wild type (blue) and *Chd7*$^{Gt/+}$ (red) mice at 4 kHz stimulus frequency. Each dot represents one animal and error bars represent standard error of the mean. (F-H) Average ABR waveforms, Wave I peak latency, and Wave I peak amplitude, for ABRs recorded with 16 kHz stimulus frequency. (I-K) Average ABR waveforms, Wave I peak latency and amplitude for ABRs recorded with 32 kHz stimulus frequency.

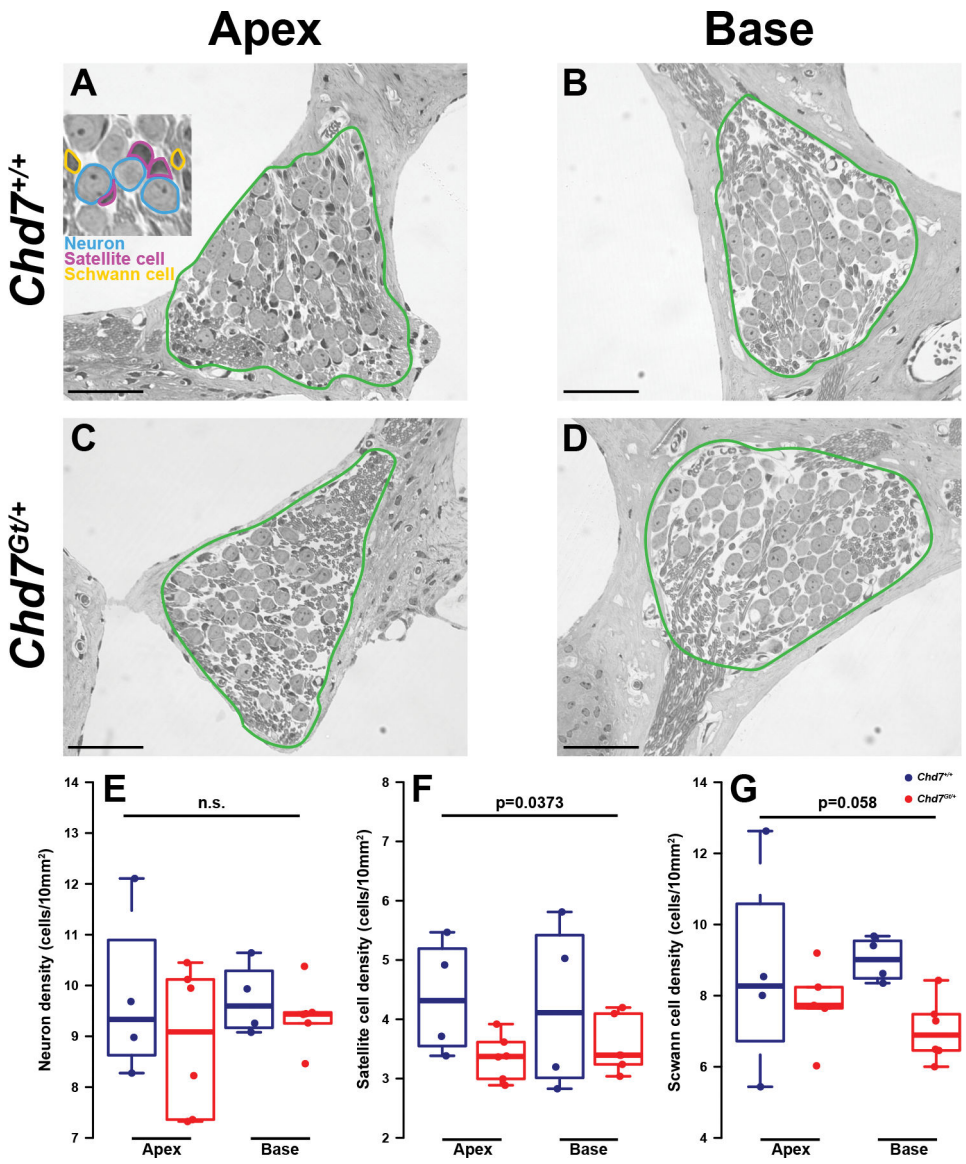

Figure 2. Reduced glial cell densities in the spiral ganglion in adult *Chd7*$^{Gt/+}$ mice.

(A, B) Representative light micrographs of spiral ganglia in the apex and base regions of the cochlea in 8-week-old wild type mice (N=4 males). Zoom-inset in A highlights the cells that were quantified: neurons (blue outline), satellite glial cells (magenta outline), and myelinating Schwann cells (yellow outline). Green outlines denote spiral ganglion area measured. (C, D) Representative images of spiral ganglia in apex and base regions of 8-week-old *Chd7*$^{Gt/+}$ cochleae (N=6 males). Scale bars in A-D represent 50μm. (E-G) Box and whisker plots of neuron (E), satellite glial cell (F), and Schwann cell (G) density in spiral ganglia of wild type (blue) and *Chd7*$^{Gt/+}$ (red) cochleae. Bold center lines of each box denote median; box border denote upper and lower quartiles. Differences in mean neuron density were not statistically significant in any region measured (denoted by n.s., two-way ANOVA), but satellite cells adjacent to neurons were significantly reduced in apex and base (p=0.0373, two-way ANOVA). Myelinating Schwann cells adjacent to nerve fibers were

reduced in *Chd7*$^{Gt/+}$ cochleae but did not reach statistical significance (p=0.058, two-way ANOVA). Scale bars: 50 μm.

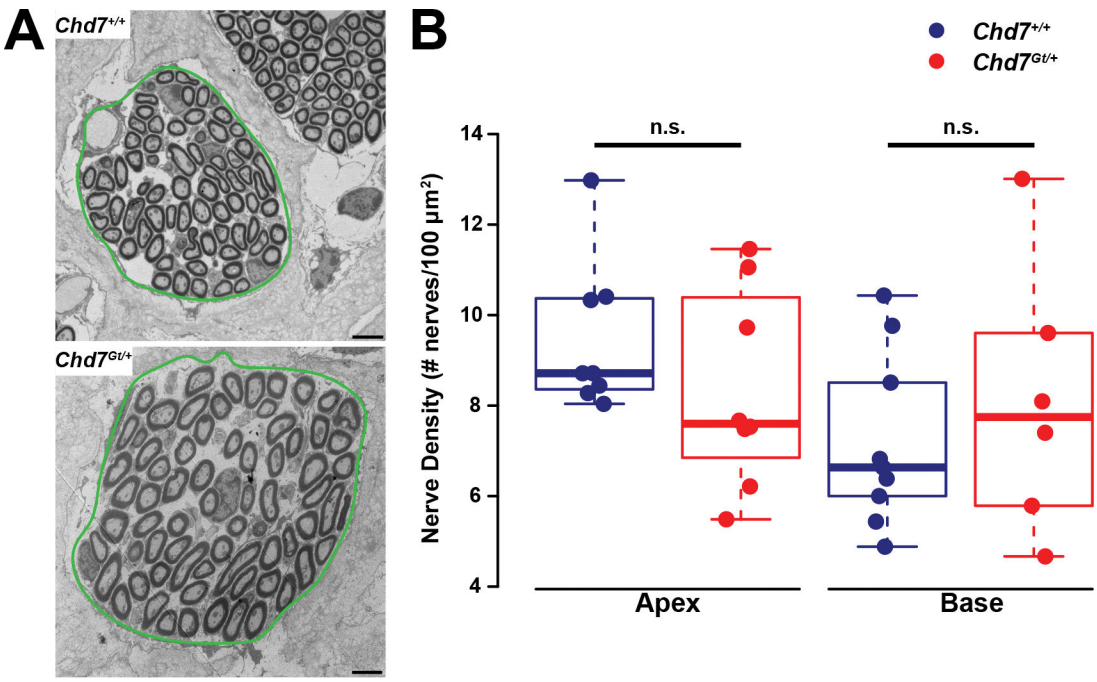

Figure 3. Density of myelinated spiral ganglion nerve fibers projecting to the organ of Corti is unaffected in adult *Chd7*$^{Gt/+}$ mice.

(A) TEM images of auditory nerve fibers in the osseous spiral lamina of wild type (top) and *Chd7*$^{Gt/+}$ (bottom) cochlear apex. Green lines demarcate the area measured to calculate nerve density. (B) Box and whisker plots of nerve density measured in the apex and base show no statistically significant difference in nerve density between wild type and *Chd7*$^{Gt/+}$ cochleae (denoted by n.s., two-way ANOVA). Bold center lines of each box denote median; box border denote upper and lower quartiles. N=8 male mice for each genotype group. Scale bar: 4 µm.

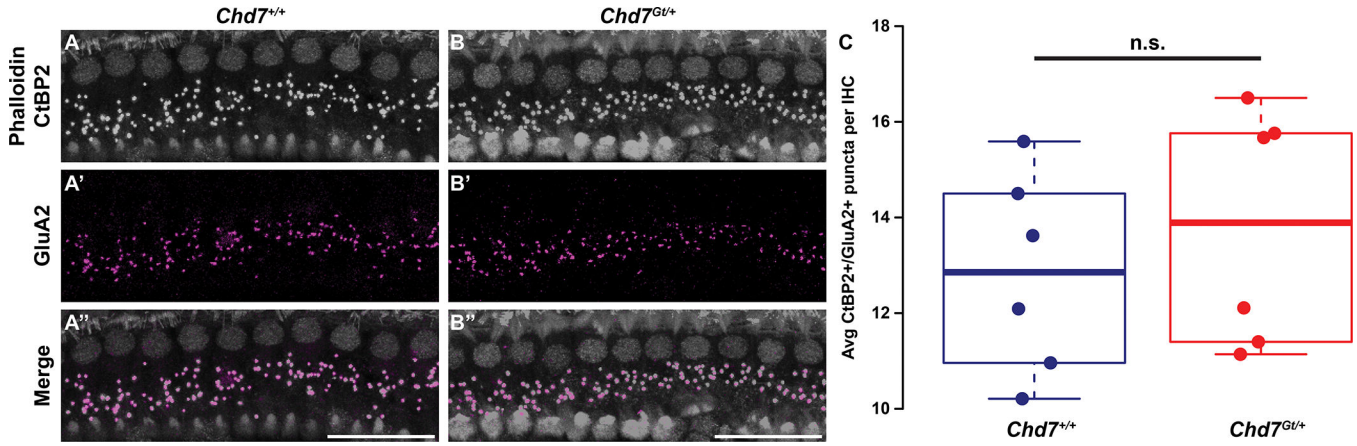

Figure 4. Inner hair cell synaptic puncta are intact in postnatal *Chd7*$^{Gt/+}$ organ of Corti.

Whole mount preparations of wild type (A-A") and *Chd7*$^{Gt/+}$ (B-B") P28 cochleae (apex) stained with Phalloidin, CtBP2, and GluA2. (C) Box and whisker plot of synaptic puncta quantification as average number of CtBP2+/GluA2+ puncta per inner hair cell. Bold center lines of each box denote median; box border denote upper and lower quartiles. No statistical significance of difference in mean is denoted by n.s. (Welch's two sample t-test). N=6 male mice per genotype group. Scale bar: 25 μm.

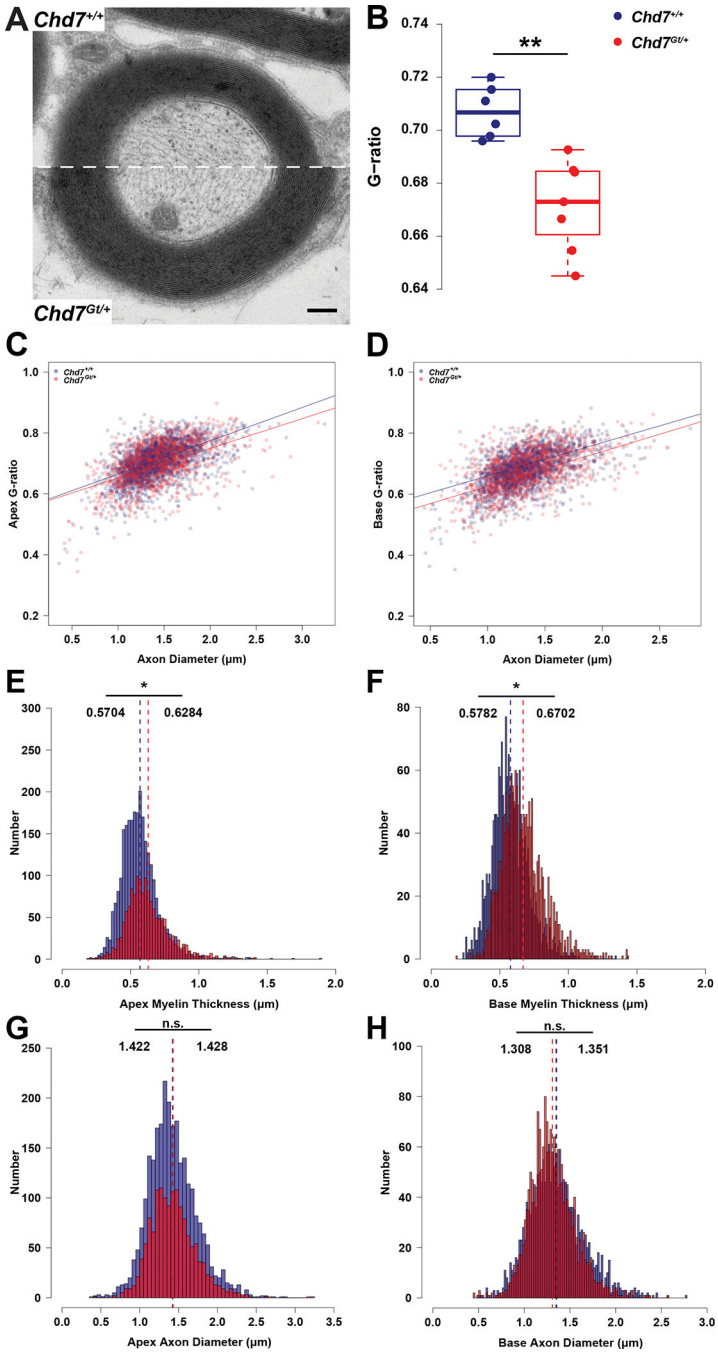

Figure 5. Subtle but significant hypermyelination of auditory nerve fibers in adult *Chd7*$^{Gt/+}$ cochleae.

(A) TEM images of spiral ganglion axons of equivalent diameter from wild type (top) and *Chd7*$^{Gt/+}$ (bottom) apical cochleae. The myelin sheath encasing the *Chd7*$^{Gt/+}$ axon is visibly thicker. (B) Box and whisker plot of mean G-ratio of each ear assessed in wild type (N=6 male) and *Chd7*$^{Gt/+}$ (N=7 male) mice. ** indicates $p < 0.001$ by Welch's two sample t-test. Bold center lines denote median; box borders denote upper and lower quartiles. (C-D) Scatter plot of G-ratio vs. axon diameter measured in wild type (blue) and *Chd7*$^{Gt/+}$ (red) spiral ganglia in apex (C) and base (D) of the cochlea. Linear regression analysis shows

decreased G-ratio in *Chd7*$^{Gt/+}$ mutants compared to wild type controls in both apex and base regions. (E-H) Histograms of distribution of apex myelin thickness (E), base myelin thickness (F), apex axon diameter (G), and base axon diameter (H) of axons measured to compute G-ratios. Myelin thickness is significantly increased in *Chd7*$^{Gt/+}$ apex and base spiral ganglion axons, while axon diameter is not significantly different. * denotes $p < 0.05$. by two-way ANOVA. Scale bar: 200 nm.

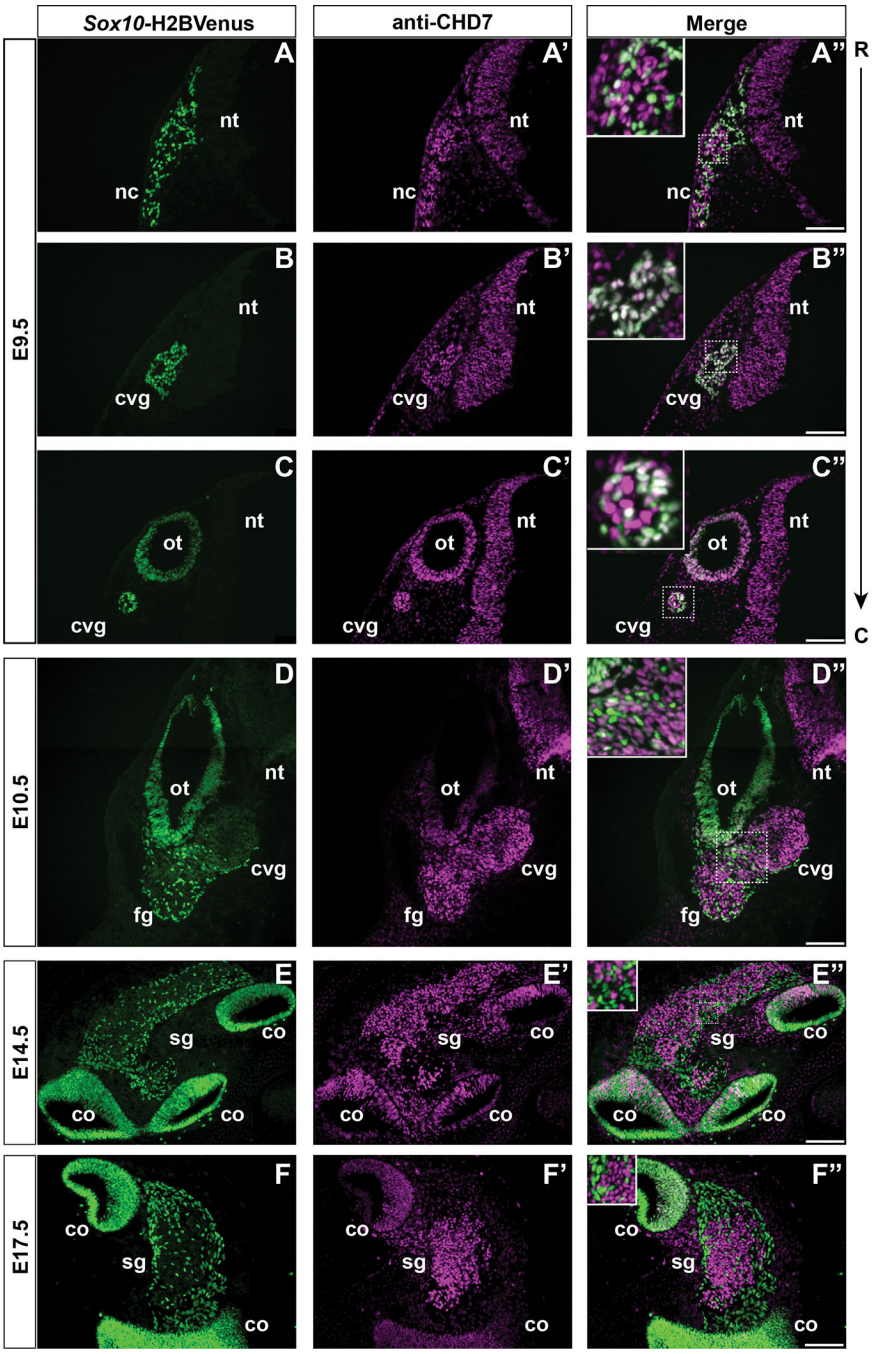

Figure 6. *Chd7* is transiently expressed in a subset of Schwann cell precursors in the cochleovestibular ganglion but absent in glial cells in the developing and mature spiral ganglion.

Transverse cryo-sections of *Sox10*-H2BVenus (green) transgenic embryos stained with anti-CHD7 antibody (magenta). Staining at E9.5 shows robust expression of CHD7 in *Sox10+* migratory neural crest cells (NCCs) rostral to the otocyst (A-A"), as well as in *Sox10+* NCCs populating the cochleovestibular ganglion (cvg) rostral to the otocyst (ot) (B-B"). CHD7 is also expressed in the caudal portion of the cvg, but in a mosaic pattern (C-C"). Arrow on the right side indicates the rostral to caudal presentation of panels A-C. By E10.5, CHD7 expression within the cvg is mostly restricted to *Sox10*- cells, with few remaining

double-labeled cells (D-D”). By 14.5 (E-E”) and continuing through E17.5 (F-F”), CHD7 and *Sox10*-H2BVenus are mutually exclusive in the cochlear spiral ganglion (sg) while CHD7 remains high in the cochlea (co) and *Sox10*- cells. Staining was conducted on a minimum of 3 sections from 3 embryos for each age group. Scale bar: 100 μm.